Chapter 10

Electrochemical Anodic Oxidation of Organic Compounds Coupled with the Cathodic Production of Molecular Hydrogen

Abstract

A Bi-doped TiO_2 anode, which is prepared from a mixed-metal oxide coating deposited on Ti metal, coupled with a stainless steel cathode is shown to be efficient for conventional water splitting. In this hybrid photovoltaic/electrochemical system, a photovoltaic (PV) cell is used to convert solar light to electricity, which is then used to oxidize a series of phenolic compounds at the semiconductor anode to carbon dioxide, with the simultaneous production of molecular hydrogen from water/proton reduction at the stainless steel cathode. Degradation of phenol in the presence of a background NaCl electrolyte produces chlorinated phenols as reaction intermediates which are subsequently oxidized completely to carbon dioxide and low-molecular-weight carboxylic acids. The anodic current efficiency for the complete oxidation of phenolic compounds ranges from 3 to 17%, while the cathodic current efficiency and the energy efficiency for hydrogen gas generation ranges from 68 to 95% and from 30 to 70%, respectively.

Introduction

Hydrogen is under consideration as a viable alternative and renewable energy source. This is partially due to the increasing price of fossil fuels and a growing demand for fuels that are carbon-free and therefore environmentally benign[1–3]. In the United States alone, the hydrogen market was estimated to have an economic value of $798 million in 2005; this number is expected to rise to $1,600 million in 2010[3]. Hydrogen is produced primarily by steam-methane reformation (SMR). SMR accounts for 95% and 48% of all hydrogen produced in the U.S. and in the world, respectively. However, the SMR process has a large carbon footprint in the form of carbon dioxide and carbon monoxide emissions. For example, the carbon released during SMR is 2.5 times by mass greater than the hydrogen produced.
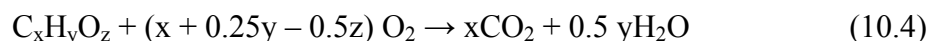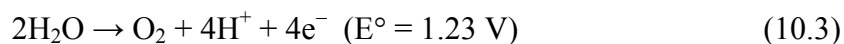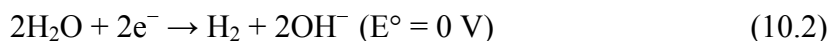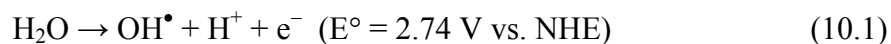
Electrochemical water splitting (i.e., electrolysis) provides a zero-carbon alternative to SMR. However, the major component of the cost of electrolytic hydrogen production is not the energy efficiency, but the price of electricity. In this regard, the U.S. Department of Energy (DOE) has established a target energy efficiency of 76% (corresponding to $2.75/GGE H_2) for electrolytic hydrogen generation (e.g., alkaline electrolyzers or proton exchange membrane electrolyzers) by 2015. The current average for commercial electrolyzers is 62%[4]. In order to reduce the overall cost of the electrolysis, low-cost, renewable energy sources, such as solar light, should be utilized as an energy source. Alternatively, the overall costs could also be reduced by implementation of a dual-purpose electrolytic system that couples hydrogen generation with energy-intensive water or wastewater treatment.

The underlying concept of solar-light driven (PV) electrolysis for hydrogen production has been previously suggested and evaluated[5–9]. The primary objective is to produce hydrogen as a storable fuel of high energy density for the dark generation of electricity. This approach is an alternative to a battery-based storage system. However, the PV-electrolyzer-hydrogen systems were determined to be economically impractical as compared to the PV-electricity-battery systems, due to inefficiencies of converting electrons to hydrogen. Thus it is suggested to simultaneously treat wastewater by electrolysis to improve overall energy efficiencies. Hybrid systems which electrolytically produce hydrogen while simultaneously oxidizing organic substrates have also been reported[10–12]. However, the previously reported systems operate noncatalytically, with much lower efficiencies, and require severe conditions (e.g., pH < 2, molar ranges of reagents), making them nonpractical.

Therefore, in order to address the goal of PV-driven electrolytic hydrogen production with simultaneous oxidation of wastewater constituents, we have combined a stainless-steel (SS) cathode for reductive hydrogen production with a Bi-doped TiO_2 anode for oxidative organic destruction. It was determined that the hybrid electrolysis system operates catalytically (addition of organics increases H_2 production efficiencies) under mild conditions (50 mM salt) with relatively high efficiencies (30% to 70% H_2 energy efficiencies).

The details of the electrochemistry give insight into these processes. The anode generates oxidizing radical species (e.g., $OH^\bullet$, $Cl^\bullet$) (eq. 10.1), which subsequently react with aqueous pollutants while the cathode splits water into hydrogen (eq. 10.2). Oxygen evolution via water oxidation (eq. 10.3) is normally the complementary reaction to H_2

production (eq. 10.2) and thus the generation of radical species (eq. 10.1) at the anode results in nonstoichiometric water splitting (i.e., $H_2/O_2 > 2$).

$$H_2O \rightarrow OH^{\bullet} + H^+ + e^- \quad (E° = 2.74 \text{ V vs. NHE}) \qquad (10.1)$$

$$2H_2O + 2e^- \rightarrow H_2 + 2OH^- \quad (E° = 0 \text{ V}) \qquad (10.2)$$

$$2H_2O \rightarrow O_2 + 4H^+ + 4e^- \quad (E° = 1.23 \text{ V}) \qquad (10.3)$$

$$C_xH_yO_z + (x + 0.25y - 0.5z) O_2 \rightarrow xCO_2 + 0.5 \, yH_2O \qquad (10.4)$$

Previously, we developed a Nb^{4+}-doped polycrystalline TiO_2 anode, which generated hydroxyl radical via one-electron oxidation of water at average current efficiencies of 50%[13-16]. However, a newer, more robust, and longer lived semiconductor anode based on a mixed metal oxide of BiO_x-TiO_2 has been developed. This anode operates at current efficiencies in the range of 20 to 30%[17]. In this study, a BiO_x-TiO_2 anode is coupled with stainless steel cathode and powered by a photovoltaic (PV) array to oxidize organic substrates while simultaneously generating molecular hydrogen (Scheme 10.1)[18,19]. Phenol is used as a model chemical substrate as phenolic compounds are a common contaminant present in industrial (solvents) and municipal (detergent by-products) wastewater[20,21].

Experimental Methods

Electrodes

The anode was prepared as follows: 1) A Ti metal sheet (Ti-Gr.2 sheet, 0.50 mm thick) was cleaned using SiC paper (120 to 240 grit) before coating with a sequence of substrates (Scheme 10.2a). 2) An initial metal oxide coating containing Ir and Ta oxides at an Ir:Ta = mole ratio of 0.67:0.33 is deposited and annealed to the Ti metal base. 3) A second metal oxide coating of Bi-doped SnO_2 at a Sn:Bi mole ratio of 0.9:0.1 is applied

and annealed. 4) A third layer of Bi-doped TiO_2 at a Ti:Bi mole ratio of 0.96:0.04 is applied and annealed at high temperature. 5) The final step involves the deposition of the anodically active overcoat that also contains Bi-doped TiO_2 at a Ti:Bi mole ratio of 0.9:0.1. Each successive step of coating requires a specific heat-treatment regime at different temperatures and durations. More details are provided elsewhere[17]. Two types of anode-cathode couples were used for the experiments reported herein. The first couple is composed of a single anode with an active area of contact with the electrolyte solution of 10.0×2.0 cm^2, and two-piece stainless-steel (SS) cathodes (Hastelloy C-22) of the same size on both sides (i.e., a sandwich configuration) of the Bi-doped TiO_2 anode, at a separation distance of 2 mm. The second configuration involves a small pilot-scale reactor consisting of 5 anode plates (5 pieces $\times$ 800 cm^2/piece) and 6 stainless steel cathode plates that face each other with a distance of separation of 2 mm (Scheme 10.2b).

Electrolysis Experiments

The BiO_x-TiO_2 anode and SS cathode couple was immersed in an aqueous electrolyte solution of 50 mM NaCl (200 mL or 20 L) and was stirred under continuous purging with air or nitrogen as a background carrier gas. The target substrates (e.g., phenol) were mixed in with a background electrolyte or added during the course of electrolysis. A constant cell voltage or current was applied to the electrodes with a DC power supply (HP 6263B and 6260B). For the PV-powered electrolyses, a commercial thin film, amorphous silicon PV (Silicon Solar, Inc.) with a peak power output of 6.4 W ($PV_{peak} = E_{peak} \times I_{peak}$; $E_{peak} = 8 - 10$ V; $I_{peak} = 0.95$A) and with active surface area of 1280 cm^2 was used (Scheme 9.1). Incident solar radiation was monitored and recorded with a pyranometer (Apogee) connected to a datalogger (Campbell Scientific). Cell voltage (E_{cell})

and cell current (I_{cell}) were measured by multimeters (Fluke). The current efficiencies (CEs) and the energy efficiencies (EEs) for hydrogen production (i.e., higher heating value) were obtained by the following equations 10.5–10.9

$$CE\ (\%) = \frac{\text{Number of molecules produced } (H_2, O_2, \text{ or } CO_2) \text{ or degraded (phenol)}}{\text{Number of electrons flowed}} \times n \times 100$$

(10.5)

$$\text{DC or PV-powered Electrolytic } H_2\ EE = \left(\frac{(39\ W \cdot h/g \times H_2 \text{ rate} \times 2\ g/mol)}{E_{cell} \times I_{cell}}\right) \times 100\%$$

(10.6)

$$PV_{cell} = E_{cell} \times I_{cell} \text{ (applied to the cell reactor)} \tag{10.7}$$

$$\text{Solar-to-PV}_{cell}\ EE = \left(\frac{PV_{cell}\ (W)}{\text{Solar Flux } (W\ cm^{-2}) \times \text{PV Area } (cm^2)}\right) \times 100\% \tag{10.8}$$

$$\text{Solar-to-}H_2\ EE = \left(\text{Electrolytic } H_2\ EE \times \text{Solar-to-PV EE}\right) \times 100\% \tag{10.9}$$

where n = 2 and 4 for hydrogen and oxygen production in cathodic current efficiencies (CCEs), respectively. For the anodic current efficiencies (ACEs), n = 1 for one-electron oxidation of phenol (ACE-I), and n = 14/3 for complete oxidation from carbon at phenol to carbon at carbon dioxide (ACE-II).

Analytical Procedures

The reactor was sealed from the ambient atmosphere. At a given rate, the headspace gas of the reactor was extracted with a peristaltic pump and extracted by a differentially pumped membrane inlet into a low-pressure cell with a quadrupole mass spectrometry (Balzers) via a turbo pump (Pfeiffer; 5.0×10^{-6} torr). The volume percent of various gases in the headspace was calculated assuming that the percent was directly proportional to the ion current measured by the mass spectrometer, and that the transfer of all gases through
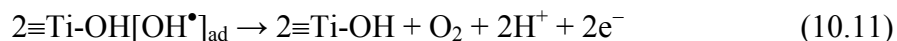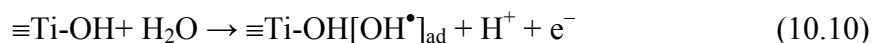
the membrane and their 70 eV electron ionization cross-sections were approximately equivalent. This assumption was validated in part since ambient air was measured to be 77% nitrogen, 17% oxygen, 5% water vapor, and 1% argon.

Aqueous organic compounds including intermediates were analyzed by a high-performance liquid chromatography (HPLC, Agilent 1100 series) with a C18 column. The eluent was composed of 55% Milli-Q water (0.1 wt% acetic acid) and 45% acetonitrile at flow rate of 0.7 mL/min. Analyte concentration was monitored by UV-Vis spectrophotometry. Total organic carbon was determined (TOC, OI Analytical Aurora Model 1030) with an autosampler (OI Analytical Model 1096).
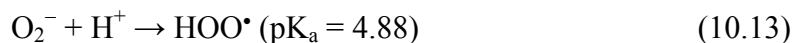
Results and Discussion

Electrolytic Nonstoichiometric Water Splitting

Figure 10.1 shows a typical DC-powered electrolysis at the BiO_x-TiO_2 anode coupled to the stainless-steel cathode couple in the presence of sodium chloride as a supporting electrolyte. Water splitting is initiated at 2.0V which is approximately 0.8 V higher than the ideal potential ($E° = 1.23$ V). The rates of H_2 production and O_2 production increase with increasing cell voltage (E_{cell}). Furthermore, cell currents (I_{cell}) also increase in a linear fashion with increasing E_{cell} above 2.1V. The rates of formation of H_2 and O_2, respectively, are 9.0 μmol/min per mA/cm^2 and 1.3 μmol/min per mA/cm^2, which correspond to nonstoichiometric H_2 to O_2 ratios between 6 and 7, depending on the specific experimental conditions. This indicates additional anodic reactions (eq. 10.1) as well as water oxidation (eq. 10.3) takes place simultaneously at the anode. Water oxidation at the surface of a semiconducting, metal oxide (MO) anode like TiO_2 is known to proceed by the coupling of two surface-bound hydroxyl radicals (eq. 10.10 & 10.11).

$$\equiv\text{Ti-OH} + H_2O \rightarrow \equiv\text{Ti-OH}[OH^\bullet]_{ad} + H^+ + e^- \tag{10.10}$$

$$2\equiv\text{Ti-OH}[OH^\bullet]_{ad} \rightarrow 2\equiv\text{Ti-OH} + O_2 + 2H^+ + 2e^- \tag{10.11}$$

The current efficiencies for the hydrogen production at the SS cathode are close to 70% while those for the oxygen production at the BiO_x-TiO_2 anode are in the range of 10 to 25% (Figure 10.1c). In spite of an initial N_2 atmosphere, H_2O_2 can be produced via superoxide/hydroperoxyl radical pathway at the cathode (eqs. 10.12 to 10.14) due to oxygen reduction.

$$O_2 + e^- \rightarrow O_2^- \text{ (at the SS)} \tag{10.12}$$

$$O_2^- + H^+ \rightarrow HOO^\bullet \text{ (pK}_a = 4.88) \tag{10.13}$$

$$2\,HOO^\bullet \rightarrow H_2O_2 + O_2 \tag{10.14}$$

The cathodic reaction 10.12 will limit the current efficiency for the hydrogen production. The energy efficiencies, which are expressed in terms of Higher Heating Value*s* (HHV) for H_2 production, are in the range of 35 to 60% (Figure 10.1d). This value decreases with increasing applied power. However, the energy efficiency can be improved, either by reducing the ohmic potential drop in the cell by increasing electrolyte concentration, or by coating noble metal (e.g., Pt) on the stainless-steel cathode.
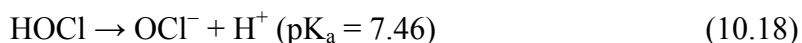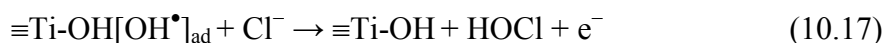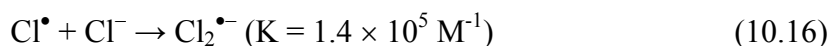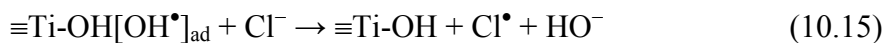
Electrochemical Oxidation of Organic Compounds

The electrochemical oxidation and complete degradation of phenol at current density of $I = 14$ mA/cm^2 is shown in Figure 10.2. Phenol is completely degraded following first-order kinetics with an apparent half-life of $t_{1/2} = 4.25$ min. The end-product of phenol oxidation, CO_2, is initially detected after 38 min of electrolysis (Figure 10.2a). Under these conditions, the H_2 production rate (i.e., 95 µmol/min) is reduced slightly to 90 µmol/min, concomitant with initiation of CO_2 production, while the O_2 production rate

remains steady at 15 μmol/min. As phenol degrades, mono-, di-, and trichlorinated phenols are formed as intermediates by stepwise chlorination of the parent phenol. The chlorinated phenols are completely decomposed within 1 h (Figure 10.2b and Scheme 10.2). When added separately, the chlorinated phenols are degraded with similar kinetics to phenol in following order of electrochemical reactivity: 2,4,6-trichlorophenol (3.74) > 2,6-dichlorophenol (1.84) > 2,4-dichlorophenol (1.38) > phenol (1.0) > 2-chlorophenol (0.78) > 4-chlorophenol (0.57). The numbers in parenthesis are observed reaction rates relative to phenol. At around 40 min of electrolysis, trichlorophenol begins to degrade rapidly (Figure 10.2a) and at the same time carbon dioxide release begins (Figure 10.2a). The total organic carbon (TOC) concentration also begins to decrease dramatically at this time (Figure 10.2c), consistent with CO_2 production. It is notable that after 2 h electrolysis the total amount of CO_2 released accounts for 25% of the initial amount of carbon present in phenol, while carbon removal based on TOC measurements is close to 34%. The "apparent carbon deficit" (~ 9%) consists of dissolved carbonate (CO_3^{2-}) and bicarbonate (HCO_3^-), which are removed by acidification prior to actual TOC measurements.

The phenol oxidation intermediates observed during the electrolytic degradation of phenol vary depending on the composition of anode surface and on the nature of the supporting electrolyte. In the case of Na_2SO_4, oxygenated or hydroxylated phenols such as catechol, hydroquinone, and benzoquinone are observed as the primary aromatic intermediates[22–26]. In contrast, for NaCl, a carbon-based anode produces chlorinated phenols as intermediates and SnO_2/Ti and IrO_2/Ti anodes produce nonchlorinated intermediates[27]. The electrolysis with NaCl as a background electrolyte is reported to

generate active chlorine species, such as chlorine radical ($Cl^\bullet$), dichloride radical anion ($Cl_2^{\bullet-}$), and hypochlorous acid/hyperchlorite ($HOCl/OCl^-$) via surface-bound hydroxyl radical mediated pathways (eqs. 10.15–10.18).

$$\equiv Ti\text{-}OH[OH^\bullet]_{ad} + Cl^- \rightarrow \equiv Ti\text{-}OH + Cl^\bullet + HO^- \tag{10.15}$$

$$Cl^\bullet + Cl^- \rightarrow Cl_2^{\bullet-} \; (K = 1.4 \times 10^5 \; M^{-1}) \tag{10.16}$$

$$\equiv Ti\text{-}OH[OH^\bullet]_{ad} + Cl^- \rightarrow \equiv Ti\text{-}OH + HOCl + e^- \tag{10.17}$$

$$HOCl \rightarrow OCl^- + H^+ \; (pK_a = 7.46) \tag{10.18}$$

The rate constants for the reaction of hydroxyl radical, chlorine radical, dichloride radical anion, and HClO with phenol are $6.6 \times 10^9 \; M^{-1}s^{-1}$,[28] $2.5 \times 10^{10} \; M^{-1}s{\text{-}}1$, $2.5 \times 10^8 \; M^{-1}s^{-1}$, and $2.2 \times 10^4 \; M^{-1}s^{-1}$ [29,30], respectively. As a consequence, phenol and its oxidation intermediates have a variety of degradation pathways, including surface-bound/free hydroxyl radicals, chlorine radicals, dichloride radical anions, hypochlorite ions, and possibly hydrogen peroxide as well.

As the current density is increased from 7 to 38 mA/cm^2, the half life ($t_{1/2}$) for phenol oxidation along with the anodic current efficiency (ACE-II) for complete oxidation of phenol carbon (formal charge -2/3) to carbon dioxide (formal charge +4) decreases (Figure 10.3). The faster phenol oxidation rates yield shorter CO_2 release phase-delays of 60 to 15 min. However, the amount of carbon dioxide released during the course of the electrolysis and the anodic current efficiency (ACE-I) for one-electron oxidation of phenol ($PhOH \rightarrow PhOH^+ + e^-$) is not altered significantly (Figure 10.3c). In addition, cathodic current efficiency (CCE) for hydrogen production is almost invariable in the range of 50 to 70%.

The initial concentration of phenol markedly affects the apparent degradation rate. The half life grows linearly with concentration over the range of 0.5 to 2.0 mM (Figure 10.4) and increases by two orders of magnitude at higher concentrations (i.e., $t_{1/2}$ = 1.28 min at 0.5 mM and $t_{1/2}$ = 150 min at 10 mM). As the concentration of phenol is increased, a greater number of reaction intermediates are produced, which in turn compete with phenol for oxidants. This should result in both a decrease in $t_{1/2}$ and a lengthening of the release onset time of carbon dioxide. The anodic current efficiency (ACE-I) is lowered somewhat to 8% at concentrations above 1.0 mM, while the ACE-II ranges from 5 to 10%. On the other hand, CCE is invariable (~ 68%) to increasing the initial phenol concentration. This indicates that anodic radical production and subsequent organic oxidation has minimal effects on the hydrogen production as long as substrates are initially present in the medium. A comparison of hydrogen production with and without organic substrates suggests addition of aqueous pollutants synergistically enhances the H_2 production rate[18,19].

The electrolytic efficiency of Na_2SO_4 vs. NaCl as background electrolyte was also compared. The phenol degradation rate in NaCl is two orders of magnitude faster than that in Na_2SO_4 (Figure 10.5). Sodium phosphate and carbonate have similar effects to sodium sulfate as background electrolytes. However, the cathodic H_2 production efficiency using Na_2SO_4 as an electrolyte is 23% greater than NaCl. When 50 mM NaCl is added to a 50 mM Na_2SO_4 solution at increasing concentrations, the phenol degradation efficiency increases while the H_2 production efficiency decreases (i.e., CCE at 50 mM Na_2SO_4 = 95%; CCE at 50 mM Na_2SO_4 + 50 mM NaCl = 73%; CCE at 50 mM

NaCl = 68%). This indicates the anode is oxidatively active during generation of chlorine radical species and suggests these chlorine radicals can interrupt H_2 production.

During the course of electrolysis of water and electrolyte alone, the pH of solution rises initially from pH 6 to 10 and then remains constant throughout. After current is removed, the pH decreases to 9.5 (Figure 10.6). In contrast, when electrolysis takes place in the presence of phenol, the pH increases initially to 11 and then decreases quickly to pH 7 after 20 min, and then remains in the circum-neutral range (~ pH 7.5) during the latter stages of electrolysis. The cathodic reduction of protons results in a rise in the measured pH. However, the progressive oxidation of phenol eventually produces organic acids such as oxalic, maleic, and formic acid, which account for the subsequent drop in pH. Eventually, these daughter acids are further degraded at the anode surface by surface-bound hydroxyl radicals to aqueous CO_2 (e.g., $CO_2 \cdot H_2O$, HCO_3^-, CO_3^{2-}) with the subsequent release of gaseous CO_2 accounting for the slight increase of the pH after 38 min of electrolysis (Scheme 10.2). This is the time that measurable CO_2 is released from the reactor (Figure 10.2a vs. Figure 10.6).

At pH 10, phenol is partially deprotonated ($pK_a = 9.98$) while the BiO_x-TiO_2 anode due to the presence of Lewis acid metals (e.g., Bi) at the surface should be positively charged despite the predominance of TiO_2 (pH_{zpc} of TiO_2 ~ 6.8). Thus, the ability of phenol to react directly at the anode surface at pH 10 is possible but the degree of interaction is unlikely to be strong. In contrast, substrates that are able to strongly adsorb to the anode via surface complexation should be oxidized quickly and immediately release CO_2 by multi-electron transfers instead of sequential one-electron transfers. This conjecture is confirmed by the results shown in Figure 10.7 for the oxidation of catechol ($pKa_1 = 9.45$;

$pKa_2 = 12.8)^{31}$. Catechol functions as a monodentate or a bidentate ligand binding at one or two surface titanol groups. Thus as soon as the electrolysis is initiated, CO_2 is immediately released from solution and continues over the 2 hour period of electrolysis. Salicylic acid ($pK_{a1} = 2.97$; $pKa_2 = 13.74$) also shows the same behavior. Both compounds have been observed to chelate TiO_2 surfaces (as depicted on the right-hand side of Figure 10.7)[31,32], and multiple electrons can be transferred to the anode within seconds after the initiation of electrolysis. Nevertheless, the first-order rate constants for degradation of catechol and salicylic acid are lowered by approximately 50% compared to phenol ($k_{catechol}/k_{phenol} = 0.59$; $k_{salicylic\ acid}/k_{phenol} = 0.41$). In the case of phenol, oxidation primarily occurs on homogeneously distributed phenol molecules (and intermediates) in the bulk solution, whereas in the cases of catechol and salicylic acid, the oxidation preferentially occurs to the adsorbed molecules rather than the ones remaining in the bulk. This should result in immediate and complete oxidation of the adsorbed phenol molecules, but a slower oxidation rate of the phenol molecules in the bulk solution.

Solar Powered Electrolysis and Scale-Up

Figure 10.8 shows the hydrogen production and organic oxidation results of a PV-driven hybrid reactor system under two different solar light irradiation conditions. The total incident solar light radiation energy of A ($\mathbf{I}_{S,B}$) is measured at 0.107 ± 0.005 W/cm^2, while that of B ($\mathbf{I}_{S,A}$) is around 0.100 ± 0.005 W/cm^2. The overall reaction scheme is similar to that in Figure 10.2a. As soon as the PV is connected to the electrode couples, hydrogen and oxygen are produced and phenol is degraded, following apparent first-order kinetics. Carbon dioxide is released during the latter stages of the electrolysis. The difference of incident solar energy only affects the rate of hydrogen production; the

phenol degradation rate, the oxygen generation rate, and the carbon dioxide release time-delay are almost invariable. At the condition B, the energy efficiency for the hydrogen production is around 30%. According to manufacturer, a theoretical maximum power of the PV_{peak} is 6.4 W corresponding to 4.5% of the average solar light radiation energy ($\mathbf{I}_{S,0}$ = 1100 W/m^2). However, when the PV is directly connected to the electrode couple, the power applied to the electrolysis (PV_{cell}) was 3.5 W (3.9V×0.9A). This corresponds to 55% of the PV_{peak} and 2.5% of the $I_{S,0}$.

To investigate the effect of solar flux on the PV power and the H_2 production, the PV-connected hybrid reactor was tested on a cloudy day. As shown in Figure 10.9, $\mathbf{I}_S$, E_{cell}, and I_{cell} vary over the range of 0.1 W/cm^2 to 0.08 W/cm^2, 4.1 V to 3.7 V, and 0.7 A to 0.9 A, respectively. The $\mathbf{I}_S$ continually decreases over the period of time from 15 min to 50 min of electrolysis, and the PV_{cell} and the H_2 production rate also follow the trend. However, upon addition of phenol to the reactor at 52 min, the H_2 production rate substantially increases in spite of a continued decrease in $\mathbf{I}_S$ and PV_{cell}. The H_2 production rate begins to decrease again after reaching a rate maximum of ~ 0.21 mmol/min. This behavior was observed again after a subsequent phenol addition at around 80 min. The synergistic effect of phenol addition on H_2 production efficiency has been qualitatively described elsewhere[18]. Briefly, oxidants such as $HO^\bullet$, $Cl^\bullet$, $Cl_2^{\bullet-}$, and $HClO/ClO^-$ produced at the anode can act as electron shuttles consuming electrons at the cathode. Reactive oxidant reduction is thermodynamically favored over proton/water reduction. When organics such as phenol are added to the system, they consume oxidants and a greater fraction of cathodic electrons are available for proton/water reduction. Our

observations show this can increase H_2 production energy efficiencies by as much as 30 to 53% at low I_{cell}.

The PV_{cell} is correlated to the $\mathbf{I}_S$ with and without phenol addition (Figure 10.10a). Without phenol addition (i.e., pure electrolysis), the PV_{cell} efficiency (= $PV_{cell}/\mathbf{I}_S \times 100\%$) is determined to be 2.0 to 2.8 %. The lower efficiency than supplier-reported (PV_{peak} = 4.5%) is probably due to overestimation of the array performance by the supplier and a conversion efficiency loss by the heating of the array and ohmic drop within the reactor[33]. The PV_{cell} efficiency increases linearly by 1.5 times from 2.37% to 3.58% by addition of phenol. The presence of phenol molecules also affects the electrolytic H_2 energy efficiency and behavior. As PV_{cell} increases in the absence of organics, the electrolytic H_2 production increases linearly with an average efficiency of 22% (= H_2 energy/PV_{cell} in Figure 10.10b). However, in the presence of phenol, the H_2 production energy efficiencies do not correlate with PV_{cell}. Prior to phenol addition, the electrolytic H_2 energy efficiency is around 20%. After phenol addition, PV_{cell} decreases to 2.1×10^{-3} W/cm^2 and H_2 production efficiencies increase to nearly 40%. The overall solar-to-H_2 energy efficiency (= H_2 energy/$\mathbf{I}_S \times 100\%$) also displays a similar trend. In the absence of phenol, the overall efficiency is around 0.67% (Figure 10.10c). The addition of phenol increases the overall efficiency from 0.53% (5.5×10^{-4} W cm^{-2}/ 1.03×10^{-1} W cm^{-2}) to 1.0% (8.1×10^{-4} W cm^{-2}/8.1×10^{-2} W cm^{-2}), which is similar to the efficiency observed in Figure 10.8.

For evaluation of a sub-pilot scale electrolysis, a 20 L batch reactor was prepared using 5 anodes (each, 800 cm^2) and 6 cathodes of the same dimensions arranged in an alternative fashion (Scheme 10.2b). At a total power of 60 W (3 V×20 A), carbon

dioxide production is observed after 20 min, and the hydrogen production rate is 3.5×10^{-3} mol/min with an energy efficiency of 28% (Figure 10.11a). The degradation half-life of 1 mM phenol is < 2 min. Based on these operation conditions, we can estimate the PV area required (i.e., PV_{cell} efficiency = $PV_{cell}/(I_{S,0} \times PV$ area$) \times 100\%$) to treat variable volumes of wastewater contaminated with 1 mM phenol (Figure 10.11b). It is clear that water-treatment capacity is strongly related to the PV area and efficiency. For example, treatment of 16 metric tons of water (i.e., 1.6 kg phenol) daily (i.e., operation for 9 h/day) requires a 62 m^2 PV panel operating at 10% efficiency. In addition, hydrogen is obtained as a potentially useful byproduct. Hydrogen production rates are affected both by the water treatment capacity and H_2 energy efficiency (Figure 10.11c). Small-scale reactors are usually better than large reactors for energy efficiency. At a H_2 energy efficiency of 60%, the treatment of 16 tons of water with a PV of 10% efficiency will yield around 1 kg of H_2.

Technical Consideration.

Electrodes

Commercial electrolytic water splitting typically employs Pt group metals (PGM) as anodes and Ni-based alloy (e.g., Ni-Zn, Ni-Al, Ni-Co, Ni-Mo-Cd)[34-36], stainless steel[36], or noble metals (e.g., Pt, Au) as cathodes, and operates at extreme conditions such as high electrolyte concentrations (> 1.0 mol/L), high pH (> 1.0 mol/L KOH), and high pressure. The main reason for employing the Pt-based anode is that Pt catalyzes the four-electron oxidation of water (10.3). However, for the electrochemical oxidation of organic compounds (10.4), the anode should preferentially generate surface-bound or homogeneous radical species (e.g., $HO^{\bullet}$, $Cl^{\bullet}$).

A variety of anodes, such as single metal oxides (e.g., PbO_2[24,25,37-41], SnO_2[24,37,39,42], IrO_2[42,43], RuO_2[43]), multiple metal oxides (e.g., Ta_2O_5/IrO_2[44], $Bi-PbO_2/Pt$[40], PbO_2/SnO_2[45], $IrO_2/RuO_2/TiO_2$[46]), and boron-doped diamond (BDD)[47] have been utilized for the electrolytic treatment of aqueous chemical contaminants. For example, PbO_2 coated on titanium substrate has been widely studied; however, the likely release of lead ions and long-term anodic stability issues are drawbacks to the practical application of PbO_2 anodes. The BDD electrode has also been the subject of a number of studies due to its great stability and wide potential window[47]; yet the high price of synthetic diamond hinders application even at the pilot scale. Application of Pt-based anodes is impractical due to formation of polymeric surface films during phenol oxidation, which reduces energy efficiencies[22,48,49]. In comparison, the $BiOx-TiO_2$ anode employed in this study is found to be very stable and results in decent current efficiencies in the range of 25 to 36% for oxidation of propylene glycol[17]. In addition, it has been manufactured at the sub-pilot scale with electrode areas nearing a square meter at relatively low costs. Various cathodes are available for use in combination with the $BiOx-TiO_2$ anode. From an economical point of view, SS is the most feasible in cost, stability, and availability. Surface treatment of SS (e.g., Ni or Pt-coating) may catalyze electron transfer to protons/water and increase H_2 energy efficiencies[50,51]. However, a great increase is not expected, since energy efficiencies are already in the range of 30% to 70%.

Technical Comparison

It should be noted that the PV-electrolysis-water-treatment system used in this study has many differences as compared to the commercial PV-electrolyzer systems. First, few experimental studies on hybrid PV-electrolyzer technologies for H_2 production and

organic oxidation operating at such mild conditions (atmospheric pressure, pH 6 to 11, 50 mM salt) have been reported. For example, Ahmad and Shenway evaluated a PV-driven electrolysis system for hydrogen production with reported electrolysis efficiencies of 60% (similar to our system) under much harsher conditions (27% KOH solution; ~ 4.8 mol/L; pH 14.7)[6]. Comparison of the solar-to-H_2 energy efficiency is not reliable due to different overall purpose and conditions. A high-powered and efficient PV usually has a high solar-to-H_2 efficiency. Photovoltaic arrays of 5–9 kW PV_{peak} and 8.1–8.4% PV_{cell} efficiency, coupled with alkaline electrolyzer (30% KOH) of 62 to 77% electrolytic H_2 efficiency, have overall solar-to-H_2 efficiency of 3.6 to 6.2%[33,52]. The alkaline electrolyzer of similar electrolytic H_2 efficiency (60%) has a much lowered solar-to-H_2 energy efficiency of 1.5% when coupled to a lower power PV (PV_{peak} = 53 W)[6]. Due to the extremely high electrolyte concentration, which is a usual condition for optimal efficiency during alkaline electrolysis, it is impractical for application to water treatment. In comparison, our system operates over a similar efficiency range (electrolytic H_2 energy efficiency of 30% to 70%; solar-to-H_2 energy efficiency ~ 1.0%) with a low-power PV (PV_{peak} = 6.4 W) at two-orders of magnitude lower electrolyte concentrations (2×10^{-2} to 5×10^{-2} mol/L).

Second, PV-electrolyzer systems on a lab or pilot scale have been considered and examined as alternatives to a system of PV-electricity-battery. The systems are typically composed of PV arrays for converting solar light to electricity, alkaline electrolyzers for producing hydrogen using the electricity, hydrogen storage tanks, and fuel cells for producing electricity from the stored hydrogen (and oxygen). Therefore, the primary goal of theses studies is to utilize hydrogen as a storable medium for the dark generation of

electricity. However, the PV-electrolyzer systems, which produce hydrogen, are found to be economically impractical compared to conventional PV-electricity-battery combinations. For example, total annual cost of the electricity from the electrolyze-based systems is around 3 times and 4 times higher than those of the battery-based systems due to energy losses during electrolysis and fuel-cell processes[8]. The hydrogen produced from a typical PV-electrolyzer system is also more expensive than SMR. On the other hand, if the hydrogen production can be combined with costly wastewater treatment, then PV-electrolyzer systems may become economically viable[53,54].

This hybrid system should be distinguished from reported electrochemical hybrid systems for hydrogen production and chemical oxidation in terms of practical operation and efficiency. Most hybrid systems operate with limited number of organic chemicals at lower efficiencies. For example, the DC-powered electrolytic hydrogen production from methanol was reported, but the system only works with methanol (i.e., a reversed direct methanol fuel cell process)[12]. A hybrid system of electro-assisted photo-Fenton oxidation and cathodic hydrogen production was described, yet the system operates only for a limited number of substrates under limited conditions and needs post-electrolysis treatment to separate the consumed reagents[10]. In contrast, our system has been proven to decompose and mineralize a variety of phenolic compounds (e.g., phenol, mono-, di-, trichlorinated phenols, catechol, hydroquinone, resorcinol, salicylic acids, etc.), aliphatic acids (e.g., maleic acid, malonic acid, oxalic acid, fumaric acid, polypropylene, etc.), and dyestuffs (methyl orange, ortho-methyl red, para-methyl red, methylene blue, acid orange 7, rhodamine B, etc.)[18,19]. These chemicals are commonly found in industrial and domestic wastewaters.

Application

Some issues would limit the applications of the presented hybrid system to a conventional water treatment facility. First the electrolyte (i.e., NaCl), which is intrinsically necessary for the electrolysis. However, the sodium chloride is the most abundant constituent of a water/wastewater stream, in the range 1 to 9300 kg/day[21], and wastewater inflows have a high conductivity in the range of 620 to 3550 μS/cm[55]. In addition, this hybrid is found to work efficiently even at 21 mM NaCl (~ 1.2 g/L)[17]. The other is that the electrolysis could produce some toxic byproducts. However, no chlorinated gases such as methyl chloride, dichloromethane, chloroform, tetrachloride, phosgene, vinyl chloride, or chlorine were detected during the electrolysis in the presence of phenol. The chlorinated phenols produced are very rapidly converted to carbon dioxide (e.g., $k_{2,4,6\text{-ClPhOH}} / k_{PhOH} > 3.7$), water, and chloride.

Separation and purification of the evolved gas stream is absolutely necessary. However, it is not a difficult challenge. Proton-exchange membranes such as Nafion or porous ceramic separators (e.g., fine glass frit) can be put between the anode and cathode. Since oxygen and carbon dioxide are produced at the anode, both gases are effectively separated from hydrogen produced at the cathode provided that there is an appropriate membrane separating the two compartments. In addition, even if hydrogen is mixed with carbon dioxide, CO_2 can be readily removed just by chemical absorption process (e.g., flowing carbon dioxide gas through amine solution), which is a typical CO_2 separation process in gas turbine power plants.

Current water and wastewater treatment plants involving a series of water treatment processes include pre-treatment steps to screen out solid debris and large particle

suspended solids, physical separation such as small particle coagulation, flocculation and sedimentation, floatation and clarification, biological treatment for removal of biological oxygen demand, and advanced oxidation treatment such as UV/ozone process for disinfection and reduction of chemical oxygen demand. Therefore no unit process itself could replace the overall wastewater treatment processes. Our PV-electrolytic system would replace conventional UV/ozone steps as an advanced oxidation or disinfection alternative.

Figures

Figure 10.1. Time profiles of a DC-powered hydrogen and oxygen production rate. A) As a function of cell voltage (E_{cell}) at BiOx-TiO$_2$ anode and stainless steel (SS) cathode in 50 mM NaCl solution. B) Effects of E_{cell} on cell currents (I_{cell}) and the rates of hydrogen and oxygen production. C) The rates and current efficiencies of hydrogen production and oxygen production as a function of I_{cell}. D) Effects of applied power on energy efficiencies for hydrogen production
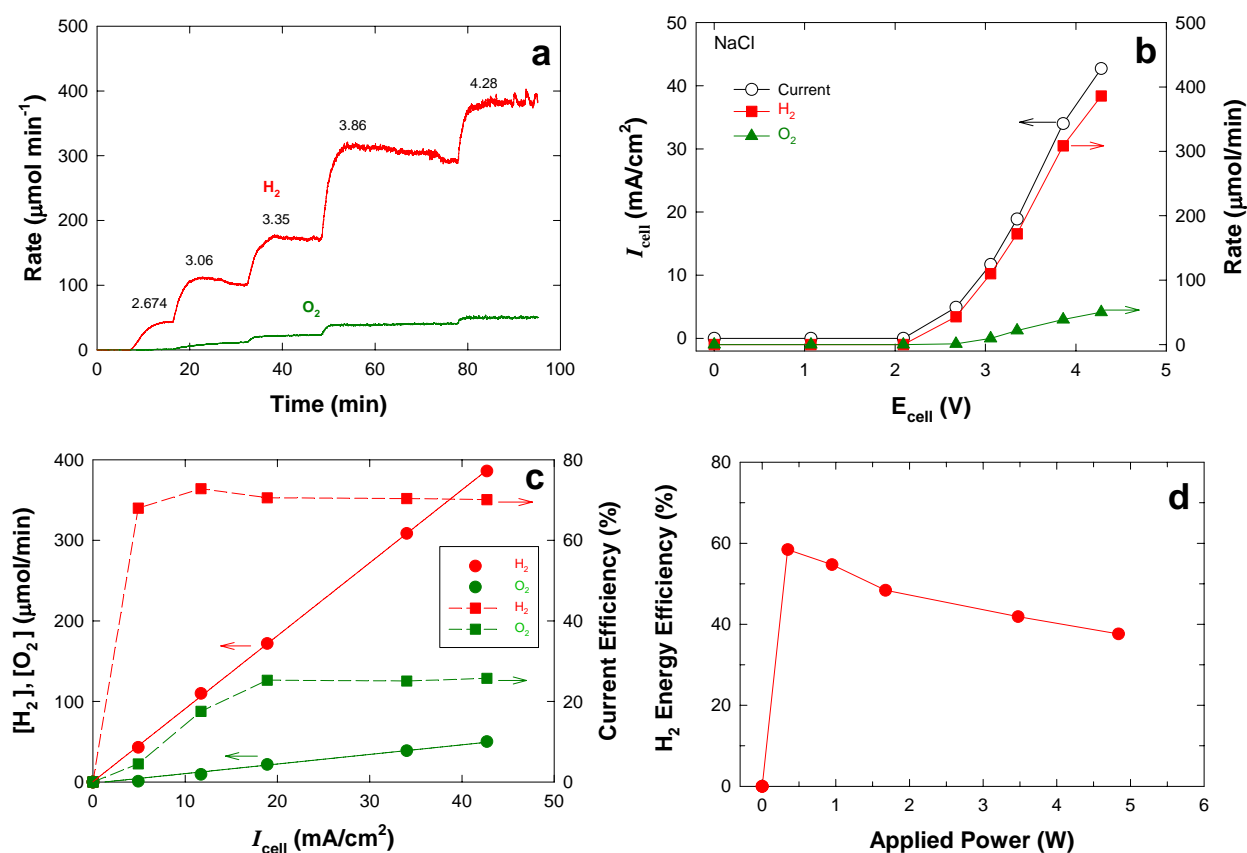
Figure 10.2. Electrochemical oxidation of phenol to CO_2 and simultaneous generation of H_2 and O_2. A) At I_{cell} = 14 mA/cm^2. B) Time profiles of intermediates generated during the oxidation of phenol. C) Time profiles of accumulation of carbon dioxide and TOC decrease. [phenol]$_0$ = 1 mM (0.2 L); [NaCl] = 50 mM; nitrogen purged continuously
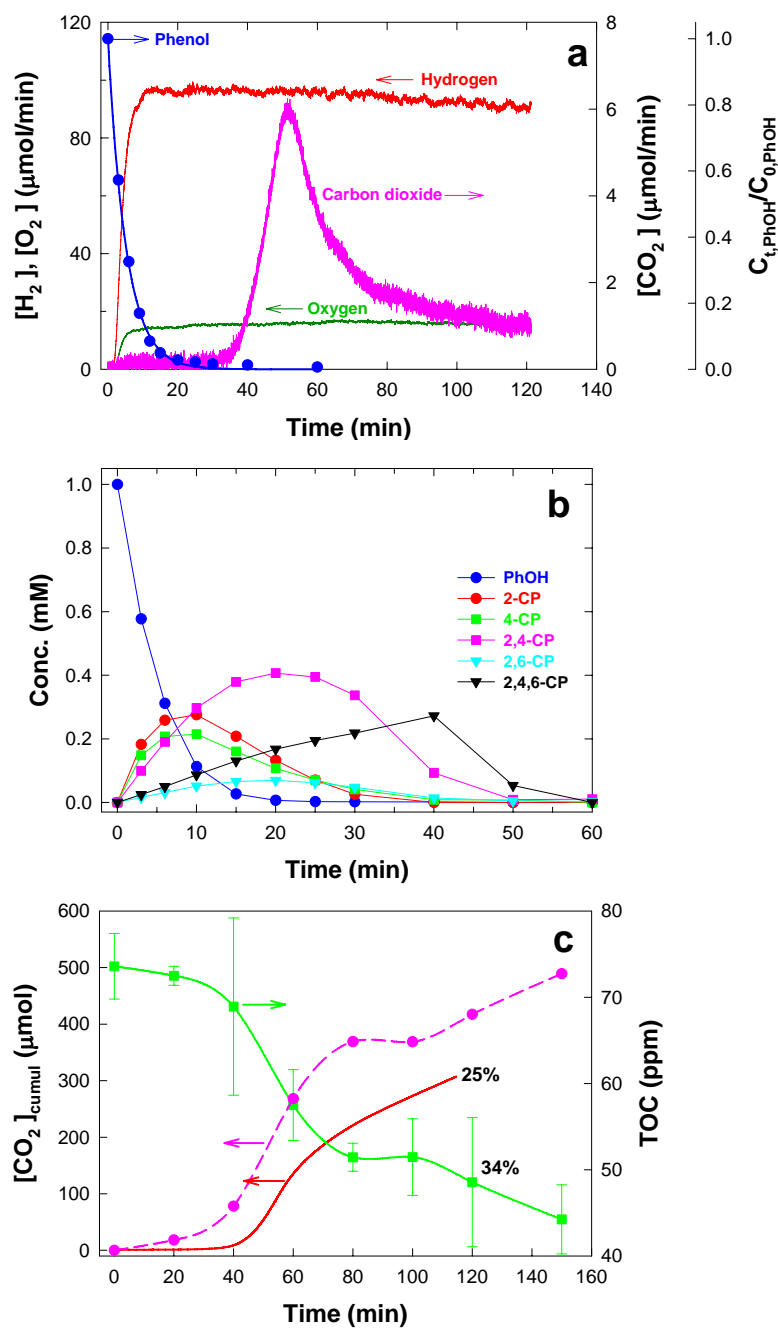
Figure 10.3. Effects of I_{cell} on observed electrochemistry. A) degradation of phenol, B) release of carbon dioxide, and C) half life time ($t_{1/2}$) for degradation of phenol, anodic efficiencies (AE-I, AE-II: see experimental section), and cathodic efficiencies (CE). Experimental conditions identical to those of Figure 10.2
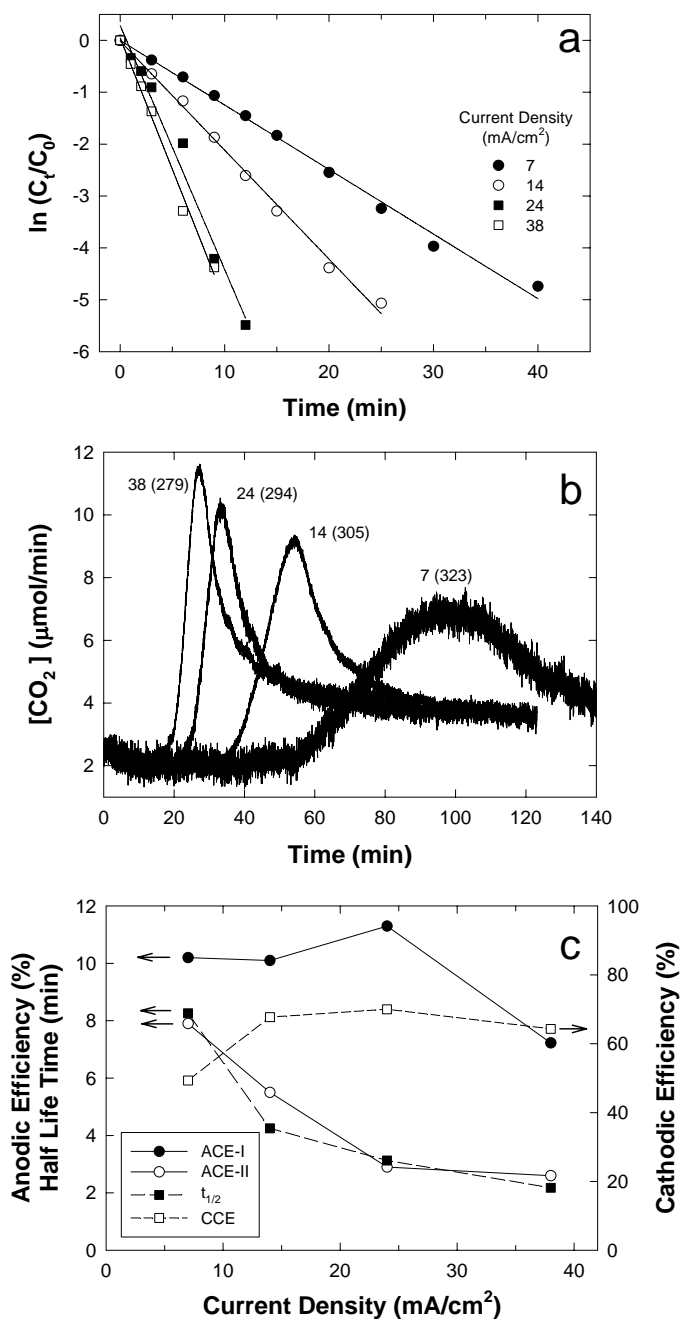
Figure 10.4. Effects of phenol concentration on electrochemistry. A) degradation of phenol, B) release of carbon dioxide, and C) half life time ($t_{1/2}$) for degradation of phenol, anodic efficiencies (AE-I, AE-II), and cathodic efficiencies (CE). I_{cell} = 14 mA/cm^2
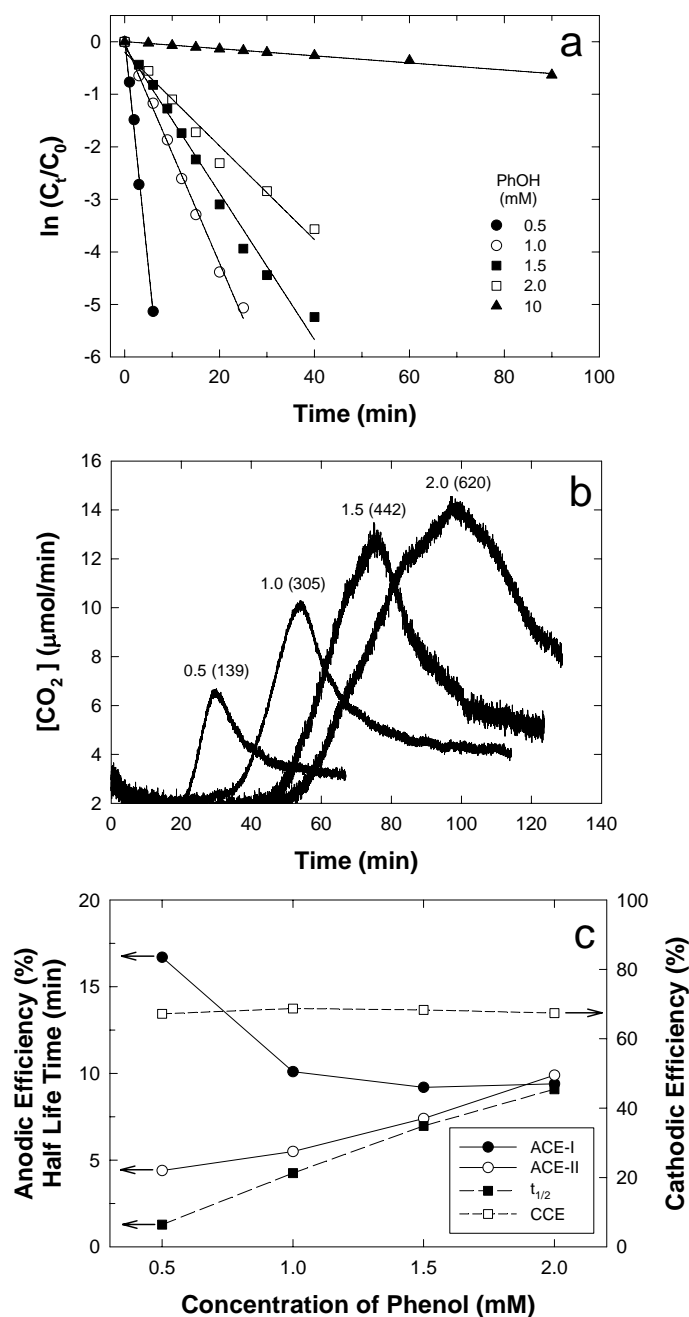
Figure 10.5. Effect of NaCl concentration on the electrochemistry. Degradation rate (k) of phenol (■) and the current efficiency for hydrogen production (●) in 50 mM Na_2SO_4. For comparison, effect of 50 mM NaCl without Na_2SO_4 was also shown for k (□) and hydrogen production (○). The current efficiency for hydrogen = (number of H_2 molecules × 2) / (number of electrons) × 100%
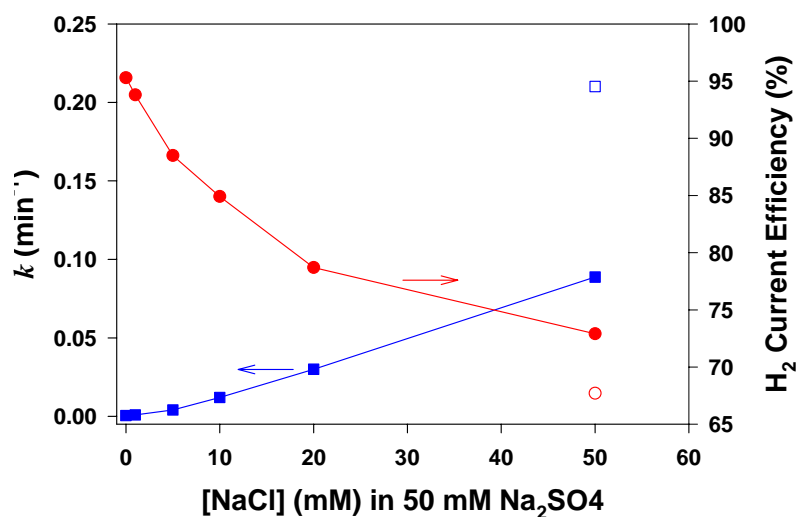
Figure 10.6. Time profiles of pH change during the course of electrolysis. I_{cell} = 14 mA/cm^2 in the absence and presence of 1 mM phenol
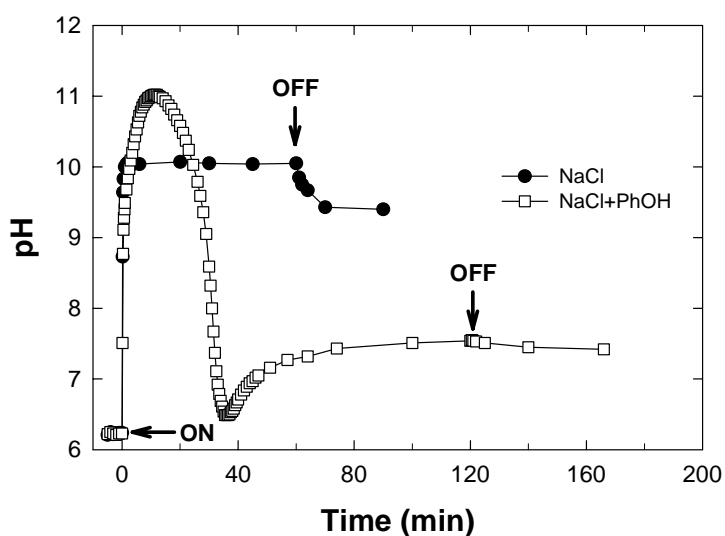
Figure 10.7. H_2 and CO_2 production during electrochemical catechol oxidation. 1 mM catechol at $I_{cell} = 12.8$ mA/cm^2
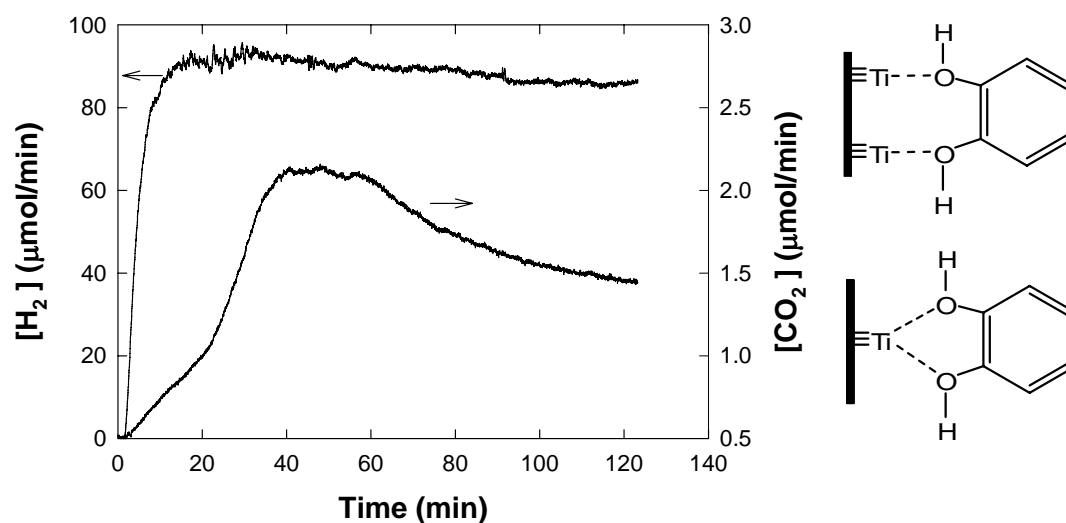
Figure 10.8. H_2 and CO_2 production during PV-electrochemical catechol oxidation. A 6.4W-rated photovoltaic cell with area of 1280 cm^2 is directly connected to the anode-cathode couple. Hydrogen A and B indicates the hydrogen production at incident solar energy of 1.00±0.01 and 1.07±0.01 W/cm^2, respectively
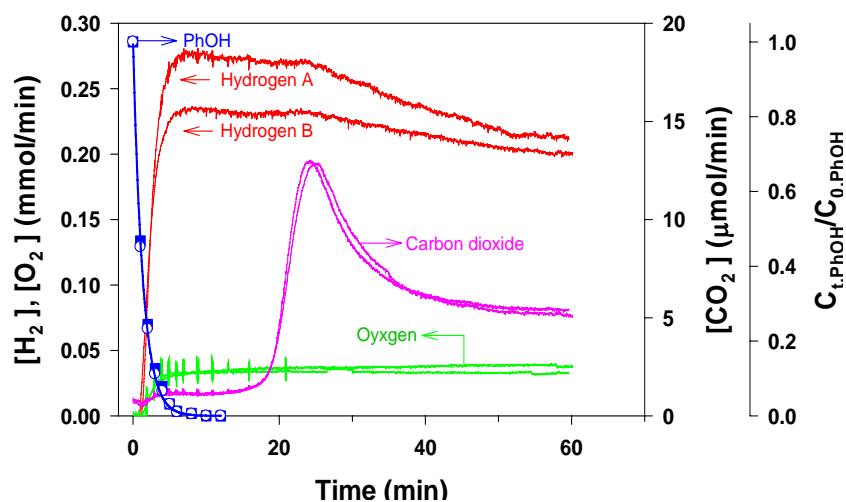
Figure 10.9. Solar-powered electrolysis with phenol addition on a cloudy day. (April 13th, 2007). A 6.4W-rated photovoltaic cell with area of 1280 cm^2 is directly connected to the anode-cathode couple. **I**$_S$: solar light radiation energy (W/cm^2); E$_{cell}$: cell voltage (V); I_{cell}: cell current (A). 1 mM phenol was successively added at 52 min and 87 min of electrolysis, as indicated by dotted lines
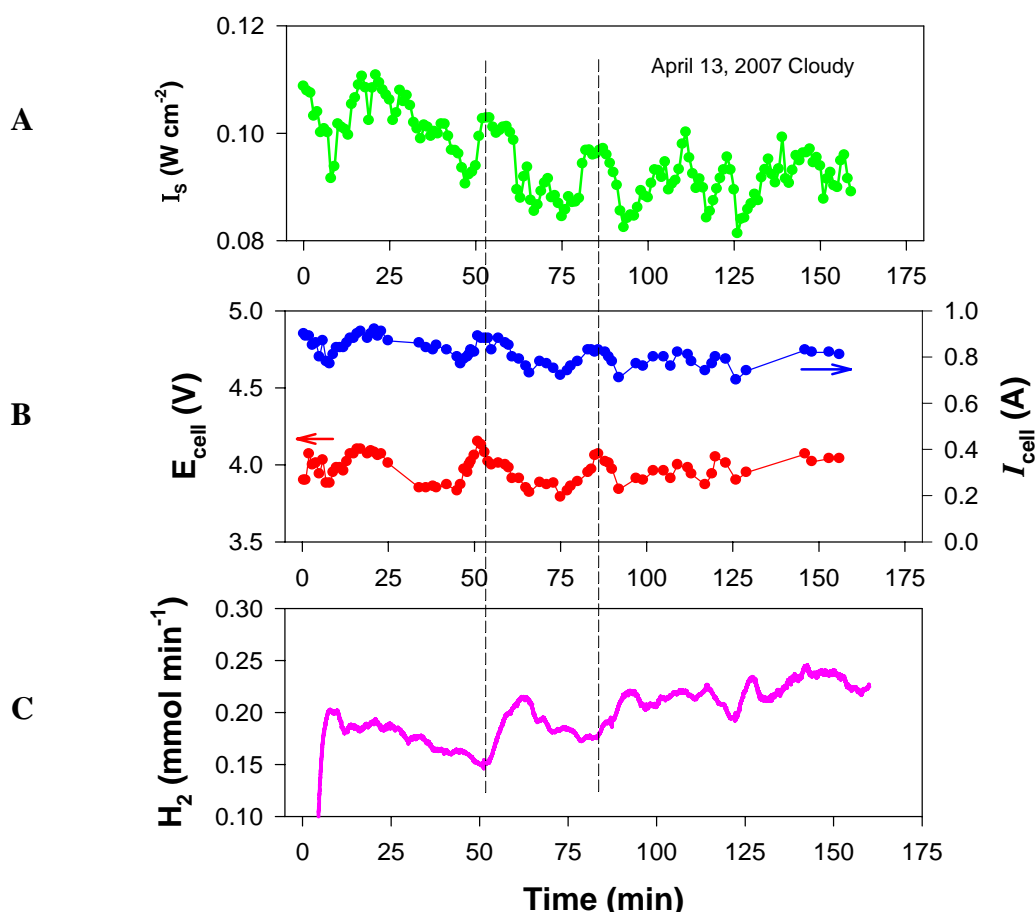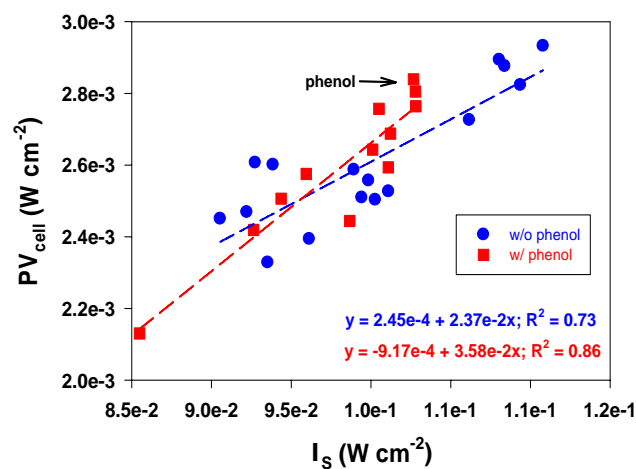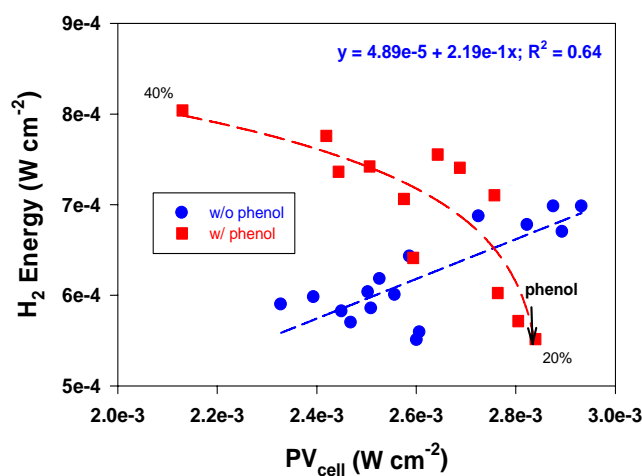
Figure 10.10. Relationships between I_S, PV_{cell}, and H_2 energy. A) I_S vs. PV_{cell} B) PV_{cell} vs. H_2 energy, and C) I_S vs. H_2 energy without and with phenol addition during electrolysis
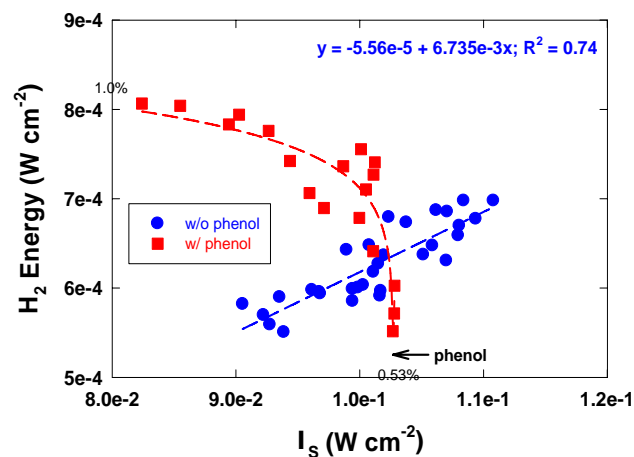
Figure 10.11. Electrolysis in a sub-pilot scale, 20 L reactor. A) A DC-powered electrochemical oxidation of phenol to carbon dioxide and generation of hydrogen in a sub-pilot scaled reactor (20L) at E_{cell} = 3V and I_{cell} = 20A. [phenol]$_0$ = 1 mM. B) Correlation between water treatment capacity and required PV area with different efficiencies. C) Effects of water treatment capacity on the amount of hydrogen obtainable with different energy efficiencies at a PV_{cell} of 10%
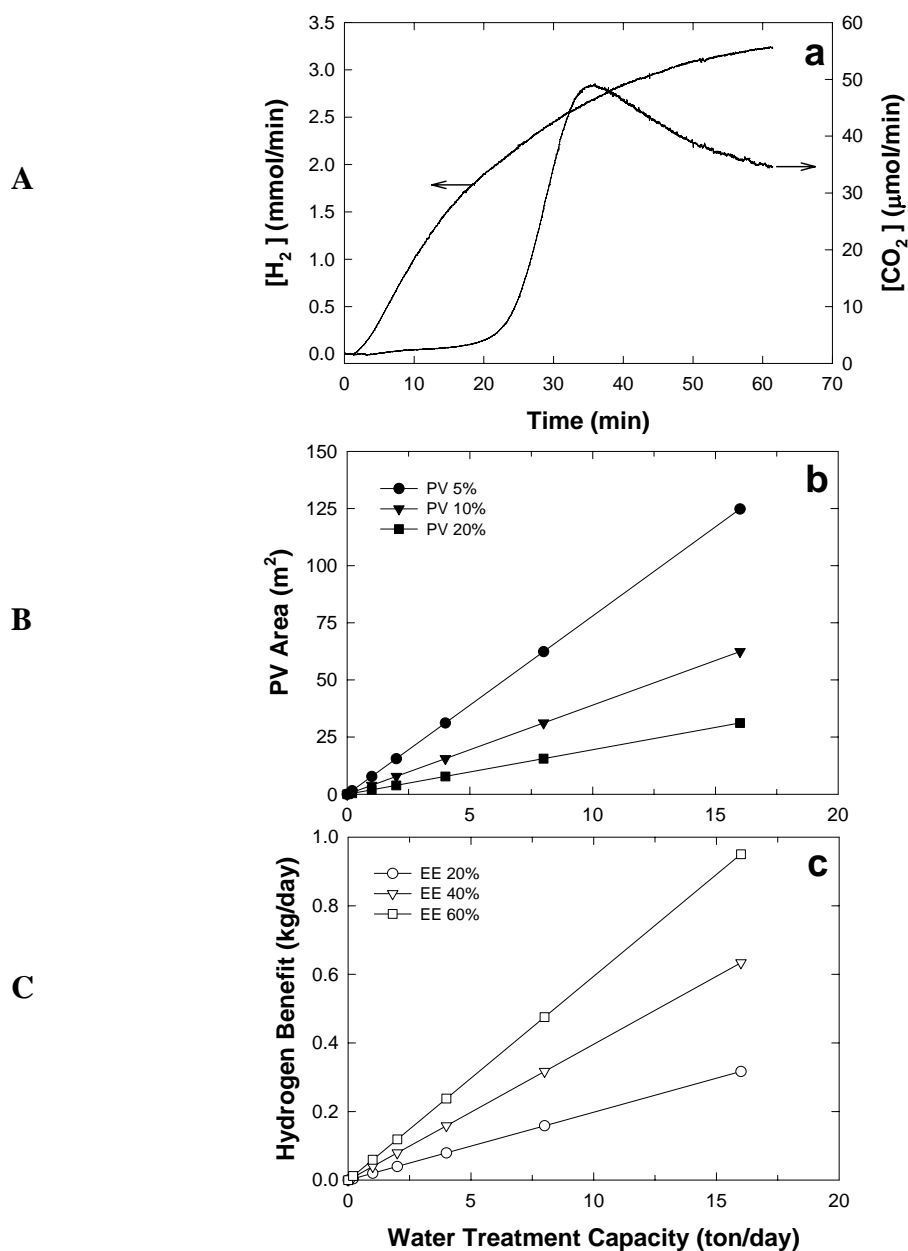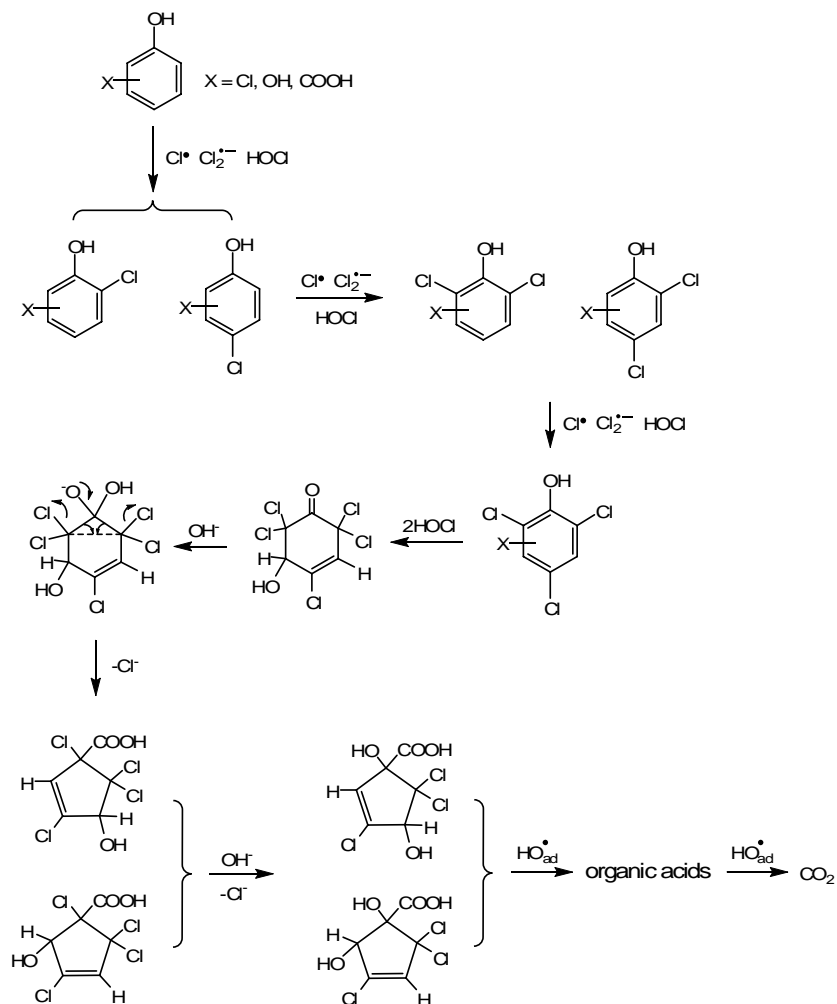
Schemes

Scheme 10.1. A) Composition and preparation procedure of BiOx-TiO$_2$/Ti anode. B) A bundle of BiOx-TiO$_2$ anode and stainless-steel (SS) cathode couples for a sub-pilot scaled electrolysis (20L)

Scheme 10.2. Proposed reaction pathway for electrochemical degradation of phenol

Tables

Table 10.1. Comparison of PV-electrolysis energy efficiencies (EEs)

PV_{peak}	Electrode	Electrolyte	Purpose	Average solar-to-PV EE[a]	Average electrolytic H_2 EE[b]	Average solar-to-H_2 EE[c]	Ref
$5\ kW_p$	-	30wt% KOH	H_2 storage & fuel cell	8.4%	62%	3.6%	Hollmuller
$53 W_p$	Ni/Ni	27wt% KOH	H_2 storage & fuel cell	-	60%	1.5%	Ahmad
$9.2\ kW_p$	Bipolar alkaline electrolyzer		H_2 storage & fuel cell	8.1%	77%	6.2%	Lehman
$6.4 W_p$	BiO_x-TiO_2/SS	0.27wt% NaCl	Hybrid	2.5%	30 – 60%	1.0%	This study

a. $PV_{cell}\ /\ \mathbf{I}_S$
b. H_2 energy $/\ PV_{cell}$
c. H_2 energy $/\ \mathbf{I}_S$

References

(1)   *International Energy Outlook 2006*; Energy Information Administration.

(2)   Penner, S. S. *Energy* **1998**, *23*, 71.

(3)   *2005 Hydrogen Market, Hydrogen R&D and Commercial Implication in the U.S. and E.U.*, available at http://www.researchandmarkets.com/reports/301714.

(4)   *Solar and Wind Technologies for Hydrogen Production*, available at http://www.hydrogen.energy.gov/congress_reports.html.

(5)   Korposki, B.; Levene, J.; Harrison, K.; Sen, P. K.; Novachek, F. *Electrolysis: Information and Opportunities for Electric Power Plants*, available at http://www.osti.gov/bridge.

(6)   Ahmad, G. E.; El Shenawy, E. T. *Renewable Energy* **2006**, *31*, 1043.

(7)   Turner, J. A. *Science* **1999**, *285*, 687.

(8)   Friberg, R. *Int. J. Hydrogen Energy* **1993**, *18*, 853.

(9)   Szyszka, A. *Int. J. Hydrogen Energy* **1998**, *23*, 849.

(10)   Soler, L.; Macanas, J.; Munoz, M.; Casado, J. *Int. J. Hydrogen Energy* **2006**, *31*, 129.

(11)   Mathieson, G.; Langdon, A.; Jamieson, G. *Dev. Chem. Eng. Mineral Process* **2006**, *14*, 71.

(12)   Narayanan, S. R.; W., C.; Jeffries-Nakamura, B.; Valdez, T. I. *Hydrogen Generation by Electrolysis of Aqueous Organic Solutions*; U.S. Patent 6,368,492; Apr. 9, **2002**.

(13)   Kesselman, J. M.; Weres, O.; Lewis, N. S.; Hoffmann, M. R. *J. Phys. Chem. B* **1997**, *101*, 2637.

(14)   Weres, O.; Hoffmann, M. R. *Electrode, Electrode Manufacturing Process and Electrochemical Cell*, U.S. Patent 5,419,824, **1995**.

(15)   Weres, O.; Hoffmann, M. R. *Electrochemical Method and Device for Generating Hydroxyl Free Radicals and Oxidizing Chemical Substances Dissolved in Water*; U.S. Patent 5,364,508; Nov. 15, 1994.

(16)   Weres, O.; Hoffmann, M. R. *Electrochemical Device for Generating Hydroxyl Free Radicals and Oxidizing Chemical Substances Dissolved in Water*; U.S. Patent 5,439,577; Aug. 8, 1995.

(17)   Weres, O. *Electrode with Surface Comprising Oxides of Titanium and Bismuth and Water Purification Process Using This Electrode*; U.S. Patent 0,000,774 A1; Jan. 4, 2007.

(18)   Park, H.; Vecitis, C. D.; Choi, W.; Weres, O.; Hoffmann, M. R. *J. Phys. Chem. C* **2008**, *112*, 885.

(19)   Park, H.; Vecitis, C. D.; Hoffmann, M. R. *J. Phys. Chem. C* **2008**, (accepted).

(20)   Glassmeyer, S. T.; Furlong, E. T.; Kolpin, D. W.; Cahill, J. D.; Zaugg, S. D.; Werner, S. L.; Meyer, M. T.; Kryak, D. D. *Environ. Sci. Technol.* **2005**, *39*, 5157.

(21)   Barber, L. B.; Murphy, S. F.; Verplanck, P. L.; Sandstrom, M. W.; Taylor, H. E.; Furlong, E. T. *Environ. Sci. Technol.* **2006**, *40*, 475.

(22)   Gattrell, M.; Kirk, D. W. *J. Electrochem. Soc.* **1993**, *140*, 903.

(23)   Canizares, P.; Martinez, F.; Diaz, M.; Garcia-Gomez, J.; Rodrigo, M. A. *J. Electrochem. Soc.* **2002**, *149*, D118.

(24)   Kotz, R.; Stucki, S.; Carcer, B. *J. Appl. Electrochem.* **1991**, *21*, 14.

(25)   Tahar, N. B.; Savall, A. *J. Electrochem. Soc.* **1998**, *145*, 3427.

(26)   Boudenne, J. L.; Cerclier, O.; Bianco, P. *J. Electrochem. Soc.* **1998**, *145*, 2763.

(27)   Korbahti, B. K.; Salih, B.; Tanyolac, A. *J. Chem. Technol. Biotechnol.* **2002**, *77*, 70.

(28)   Buxton, G. V.; Greenstock, C. L.; Helman, W. P.; Ross, A. B. *J. Phys. Chem. Ref. Data* **1988**, *17*, 513.

(29)   Hasegawa, K.; Neta, P. *J. Phys. Chem.* **1978**, *82*, 854.

(30)   Gallard, H.; von Gunten, U. *Environ. Sci. Technol.* **2002**, *36*, 884.

(31)   Araujo, P. Z.; Morando, P. J.; Blesa, M. A. *Langmuir* **2005**, *21*, 3470.

(32)   Tunesi, S.; Anderson, M. *J. Phys. Chem.* **1991**, *95*, 3399.

(33)   Hollmuller, P.; Joubert, J. M.; Lachal, B.; Yvon, K. *Int. J. Hydrog. Energy* **2000**, *25*, 97.

(34)   Los, P.; Rami, A.; Lasia, A. *J. Appl. Electrochem.* **1993**, *23*, 135.

(35)   Navarro-Flores, E.; Chong, Z. W.; Omanovic, S. *J. Mol. Catal. A* **2005**, *226*, 179.

(36)   Radhakrishnamurthy, P.; Sathyanarayana, S.; Reddy, A. K. N. *J. Appl. Electrochem.* **1977**, *7*, 51.

(37)   Rodgers, J. D.; Jedral, W.; Bunce, N. I. *Environ. Sci. Technol.* **1999**, *33*, 1453.

(38)   Bonfatti, F.; Ferro, S.; Lavezzo, F.; Malacarne, M.; Lodi, G.; De Battisti, A. *J. Electrochem. Soc.* **2000**, *147*, 592.

 (40)   Iniesta, J.; Exposito, E.; Gonzalez-Garcia, J.; Montiel, V.; Aldaz, A. *J. Electrochem. Soc.* **2002**, *149*, D57.

(41)   Kaba, L.; Hitchens, G. D.; Bockris, J. O. *J. Electrochem. Soc.* **1990**, *137*, 1341.

(42)   Comninellis, C.; Nerini, A. *J. Appl. Electrochem.* **1995**, *25*, 23.

(43)   Kim, K. W.; Lee, E. H.; Kim, J. S.; Shin, K. H.; Jung, B. I. *J. Electrochem. Soc.* **2002**, *149*, D187.

(44)   Fino, D.; Jara, C.; Saracco, G.; Specchia, V.; Spinelli, P. *J. Appl. Electrochem.* **2005**, *35*, 405.

(45)   Gherardini, L.; Michaud, P. A.; Panizza, M.; Comninellis, C.; Vatistas, N. *J. Electrochem. Soc.* **2001**, *148*, D78.

(46)   Rajkumar, D.; Kim, J. G.; Palanivelu, K. *Chem. Eng. Technol.* **2005**, *28*, 98.

(47)   Panizza, M.; Cerisola, G. *Electrochim. Acta* **2005**, *51*, 191.

(48)   Koile, R. C.; Johnson, D. C. *Anal. Chem.* **1979**, *51*, 741.

(49)   Boudenne, J. L.; Cerclier, O.; Galea, J.; VanderVlist, E. *Appl. Catal. A.* **1996**, *143*, 185.

(50)   Whalen, J. J.; Weiland, J. D.; Searson, P. C. *J. Electrochem. Soc.* **2005**, *152*, C738.

(51)   Dominey, R. N.; Lewis, N. S.; Bruce, J. A.; Bookbinder, D. C.; Wrighton, M. S. *J. Am. Chem. Soc.* **1982**, *104*, 467.

(52)   Lehman, P. A.; Chamberlin, C. E.; Pauletto, G.; Rocheleau, M. A. *Int. J. Hydrog. Energy* **1997**, *22*, 465.

(53)   *Phenolic Wastewater Treatment Alternatives*; Air Force Engineering and Service Center: Tyndall AFB FL Engineering and Services Lab, **1980**.

(54)   Jones, O. A. H.; Green, P. G.; Voulvoulis, N.; Lester, J. N. *Environ. Sci. Technol.* **2007**, *41*, 5085.

(55)   Conn, K. E.; Barber, L. B.; Brown, G. K.; Siegrist, R. L. *Environ. Sci. Technol.* **2006**, *40*, 7358.